Hydrodynamic characterisation of fire sprinkler system of a passenger railroad car.

CRAIG, M., YOUNAS, M. and ASIM, T.

2023

COMADEM
International Journal of Condition Monitoring and Diagnostic Engineering Management

Hydrodynamic Characterisation of Fire Sprinkler System of a Passenger Railroad Car

Matthew Craig [a], Muhammad Younas *[b], and Taimoor Asim [b]

[a] School of Engineering, Robert Gordon University, Aberdeen, UK (AB10 7GJ)
[b] Baker Hughes, Brent Avenue, Montrose, UK (DD10 9PB)
* Corresponding author email: t.asim@rgu.ac.uk

ABSTRACT

Fire safety is one of the major concerns in the public transport and thus passenger trains in the UK seek continuous improvement in passenger safety and comfort. In order to combat fire, there is a legal requirement in most countries across the global to install a fire suppression system within passenger railroad cars. In the event of fire, the thermal sensors trigger high pressure flow of hydrant through nozzles into the railroad car, thus supressing the fire. The efficient design of fire suppression system is highly dependent on the operational parameters of the system. The published literature, although abundant in investigating the flow characteristics through nozzles, severely lacks in conjugating this with fire suppression. Thus, in the present study, extensive parametric investigations have been carried out on the operational and design parameters of a conventional fire suppression system using an integrated approach i.e., hydrant flow and combustion. Advanced numerical techniques have been employed to evaluate the hydrodynamic characteristics of the fire suppression system based on the size of droplets of the hydrant from exiting the nozzles and the flow rate of the hydrant. The effects of these parameters on the temperature and the concentration of soot particles within the passenger railroad car have been evaluated. The results show that smaller sized hydrant droplets (250um) are more effective in supressing the fire in enclosures compared to larger droplets (750um), while higher flow rates tend to supress the fire more efficiently. It is envisaged that the results obtained in the present study will help in developing more efficient fire suppression systems for passenger railroad cars.

Keywords: Computational Fluid Dynamics; Fire Sprinkler; Railroad Car; Fire Propagation; Hydrant.

1. Introduction

Fire sprinkler systems are a proven method of suppressing the growth of compartmental fires. A study completed by the National Fire Chiefs Council (NFCC) concluded that instances of fire, where an active sprinkler system is in operation, lead to the risk of serious hospitalisation to reduce by 22% between the years 2013-2018 in the United Kingdom. Specific findings to support this is that statistic suggest that there is 30% less likely to come across smoke inhalation when fire is supressed by a sprinkler system, likewise, the risk of respiratory issues following the instance of fire is reduced [1]. However, sprinkler systems are not commonly featured within commercial passenger transport design. Manufacturers would argue that precautionary measures, which are currently in regulation alongside additional suppressants such as material selection and extinguishants, are an adequate and realistic method of reducing the risk of ignition and spread within these settings. However, in the age of heightened safety consciousness, critical examination of the key parameters of sprinkler performance would regulate design characteristics to become more complaint within these applications. Past methods of quantifying sprinkler performance include identifying time till fire containment or measuring damage to a property [2] however, by using specific key performance indicators (KPI's) such as, temperature and exhaust density would allow more accurate conclusions to be made regarding nozzle and flow design. Thus, the aim of this study is to create greater understanding using both theoretical principles and numerically investigated KPI's, which can then be used to control the onset and spread of fire more effectively and efficiently. Specifically, this research is based upon fire control within typical commercial railroad car.

Previous studies focusing on the propagation of fire within railway carriages show the criticality of such an occurrence to the safety of passengers. In both numerical based and incident review articles, it is concluded that the smoke density of combustion, caused by the materials within the carriage, poses by far the greatest risk to human injury [3,4,5]. Simply put, the lethality of the exhaust gasses cause incapacitation. It must also be considered that, the thicker the smoke, the greater the optical density and thus, the lower the visibility within in the compartment. Compartmental fires obviously enhance probability of severe human injury, when compared to open setting situations due to the reasons mentioned prior and in cohesion with smoke flow mechanics. As with all fires the smoke effluent rises vertically, as per the theory of thermal buoyancy. However due the obstruction, in this case; the roof, the smoke then travels along the roof and begins to fill the volume of the compartment from top down. This additionally compromises human life, not only as it clearly makes escape more dubious but also, would cause greater panic within the compartment; replacing any pragmatic or rational thinking people may have. It has been noted that for many burning conditions, smoke density and optical density are linearly related however, this is dependent on the chemical composition of the material fuel [6].

The role of water regarding fire suppression and attenuation is to act upon the intense thermal radiation produced by a fire and absorb the heat through its molecular content, rather than

allow the spread of heat to the environment [7]. Thus, the aim of this research is to understand how the basic properties of a sprinkler system can be manipulated to best suppress a fire within a compartmental environment. One such variable is the droplet size of each water particle. Water droplet size has an important effect on the control and suppression of temperature in compartmental fires. Previous studies have shown that finer droplet sizes, tending to a mist, both cool and stabilise a fire in faster time than conventional sprinkler systems. This is due to the fact that more heat is absorbed by the individual droplets, generating greater heat transfer [8,9]. Factors which determine droplet size within the real world are operating pressure and the size of the sprinkler orifice [10]. As dictated by Fleming [11], research data shows that droplet diameter is almost inversely proportional of the water pressure to the power 113. Likewise, it is also concluded that the droplet diameter is directly proportional to the orifice diameter to the power of 213. It must also be considered that, specific design characteristics within the nozzle can affect droplet size. Change of shape or geometry can vary water droplet diameter [12].

Previous work within this field also suggest hydrant flow rate plays a pivotal role in fire suppression. Lin et al. [13] used a numerical model to analyse a water mist sprays effect of suppression when fighting an ethanol pool fire. This study used both open and closed compartment settings. It was found that pulsing the water spray has a significant effect in terms of controlling a fire.

2. Numerical Modelling of the Passenger Railroad Car

Computational modelling of the carriage domain was carried out using Fire Dynamics Simulator (FDS) v6, which is an open-source CFD code, developed by the National Institute of Standards and Technology (NIST), designed specifically to numerically analyse the combustion mechanics and propagation dynamics of fire. Large Eddy Simulation (LES) turbulence modelling was used within the numerical code to accurately simulate the effects of flow and heat transfer by directly modelling larger eddies whilst using a sub grid scale to account for smaller eddies within the flow. This method of turbulence modelling evaluates the Navier Stokes equations in a more specific manner when compared with alternative averaging models, such as Reynolds-Averaged Navier-Stokes (RANS), whilst remaining computationally feasible [14]. One fundamental principle of LES employs is using a sub grid scale (SGS) to model smaller eddies within the turbulent effluent. This is controlled in FDS by filter width scale similarity. The algebraic relationship shown in equation 1 shows how this factor is represented within each numerical iteration. This relationship is defined by the cubic root per cell volume.

$$\bar{\emptyset}(x,y,z,t) \equiv \frac{1}{\delta x \cdot \delta y \cdot \delta z} \int_{x-\frac{\delta x}{2}}^{x+\frac{\delta x}{2}} \int_{y-\frac{\delta y}{2}}^{y+\frac{\delta y}{2}} \int_{z-\frac{\delta z}{2}}^{z+\frac{\delta z}{2}} \bar{\emptyset}(x',y',z',t)dx'dy'dz' \quad \text{Eq. 1}$$

The LES momentum transport equation is applied to the solver, in which all variables can be determined once the sub-grid stress is quantified.

$$\frac{\partial \bar{\rho}\tilde{u}_i}{\partial t} + \frac{\partial}{\partial x_j}(\bar{\rho}\tilde{u}_i\tilde{u}_i) = -\frac{\partial \bar{\rho}}{\partial x_i} - \frac{\partial \tau_{ij}^{sgs}}{\partial x_j} + \bar{\rho}g_i + \bar{f}_{d,i} + \overline{\dot{m}_b'''}\tilde{u}_{b,i} \quad \text{Eq. 2}$$

Conservation of energy is assumed within the model.

$$\rho\frac{\partial h}{\partial t} + \nabla \cdot \rho h\bar{u} = \left(\frac{\partial P}{\partial t} + \bar{u} \cdot \nabla P\right) + q''' - \nabla \cdot \bar{q} + \bar{\Phi} \quad \text{Eq. 3}$$

Net contribution of thermal radiation is calculated using the radiation transport equation for non-scattering grey gases.

$$\dot{q}_r''' \equiv -\nabla \cdot \dot{q}_r''(x) = K(X)[U(x) - 4\pi I_b(x)] \quad \text{Eq. 4}$$

$$s \cdot \nabla I(x,s) = K(X)[I_b(x) - I(x,s)] \quad \text{Eq. 5}$$

The water spray is modelled using the Langrangian method where each particle is determined to have momentum, mass and temperature and are distributed using the Roisin-Rammler-Lognormal cumulative volume fraction (CVF). This method is similar in theory and assumes that the diameter and the mass fraction of droplets are exponentially related [15,16]. Thus, this relationship is indicated in equation (6). Within this Dm represents the median diameter of each water droplet and γ is the width of the Roisin-Rammler distribution, of which FDS' default empirically driven constant of 2.4. The width of the lognormal distribution is denoted σ and its relationship to the Roisin-Rammler distribution in shown in equation (6) [17].

$$F(D) = \begin{cases} \frac{1}{\sqrt{2\pi}} \int_0^D \frac{1}{\sigma D'} e^{\left(-\frac{[\ln\frac{D'}{D_m}]^2}{2\sigma^2}\right)} dD' & (D \le D_{v,0.5}) \\ 1 - e^{\left(-0.693\left[\frac{D}{D_m}\right]^\gamma\right)} & (D \le D_{v,0.5}) \end{cases} \quad \text{Eq. 6}$$

$$\sigma = \frac{2}{\sqrt{2\pi}\cdot(\ln 2)\cdot\gamma} = \frac{1.15}{\gamma} \quad \text{Eq. 7}$$

When taking the attenuation of the water droplets into account the radiative transport equation becomes

$$s \cdot \nabla I(x,s) = -\left[K_p(x,\lambda) + \sigma_p(x,\lambda)\right] \cdot I_\lambda(x,s) + K_p(x,\lambda) \cdot I_{b,p}(x,\lambda) + \frac{\sigma_p(x,\lambda)}{4\pi}\int_{4\pi} \Phi(s,s') \cdot I_\lambda(x,s')\, ds' \quad \text{Eq. 8}$$

K_p denotes the particle absorption coefficient, σ_p is the particle scattering coefficient, $I_{b,p}$ is the emission of the particles and Φ(s, s') is the phase function of scattering. Full specification of the numerical methodology of the model is available from the FDS technical guide [18]

2.1 Model Geometry

The model was designed as such to resemble a standard passenger railroad car which would therefore allow the results of this study to be widely applicable to many carriage models. Furthermore, the criticality of the onset of fire within this setting allows a general overview to be gauged and understood on how such systems sprinkler systems should be designed within similar compartmental settings such as within commercial

aviation or cruise liners. The bounds of the computational domain were set to be 24 m x 3 m x 3 m. As depicted in Figure 1 (a) and Table 1, a total of 76 chairs were separated by an aisleway along the centreline of the compartment. Either end of the cabin was partitioned by a wall, separating the exit area and seating area, as with the general design of commercial railroad carriages. It is assumed within this study that the railroad cars walls are adiabatic. The location of the sprinkler nozzles are shown circled red within this Figure 1 (b).

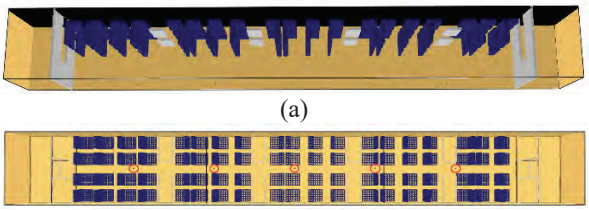

(a)

(b)

Figure 1. (a) End view of the modelled railroad car (b) Top view showing location of the sprinkler nozzle red circled.

Table 1. Dimensional characteristics of the model of railroad car

Characteristic	Dimension
Carriage length	26.5 m
Carriage width	2.825 m
Carriage height	2.8 m
Cabin length	22 m
Cabin partition wall thickness	0.4 m
Aisle width	0.468 m
Cabin door width	0.8 m
Cabin door height	1.9 m
Seating base	0.6 x 0.508 x 0.15 m
Seating back	0.15 x 0.508 x 1.016 m
Number of seating rows	19
Number of seats	76

2.2 Boundary Conditions

In order to draw conclusion on how the specifications of the sprinkler design supress fire propagation, the boundary conditions in this study were assessed around physically controllable quantities. These included adjusting the flow rate of the water between 100-300 l/min at increments of 50 l/min and varying the water droplet diameter between 250-750 µm at increments of 125 µm. This lower limit (≥ 200 µm) maintained the integrity of the 'sprinkler system' instead of fitting the criterion of a fine mist [19]. To appropriate this within a real word scenario, it is suggested that the flow rate variation is controlled by altering the water pressure within the system whilst the droplet diameter can be controlled by varying nozzle geometry within the fluid flow path. Within reality, altering the pressure would cause an effective change in water droplet diameter and vice-versa, and as such, this investigation has been conducted so that one of these variables is fixed to give a full appreciation of the suppression effect of each variable [20,21].

Table 2. Specification of the boundary conditions

Condition	Quantity
Environment	
Heat Release Rate	50 kW
Fire Location	Centre of carriage at z= 0 m
Pressure	1 atm
Ambient Temperature	20 °C
Seating Material	Polyurethane Foam with Nylon Lining [3]
Sprinklers	
Offset	0.05 m
Spray Angle	50, 80 °
RTI	40 √m/s
Activation Temperature	64 °C
Location	x= 5.33, 8.66, 12, 15.33, 18.66 m y= 1.5 m z= 3 m
Droplet Diameter	750, 625, 500, 375, 250 µm
Flow Rate	300, 250, 200, 150, 100 l/min

Sprinklers within this research respond to a response time index (RTI) which is a specification of the sprinkler. According to BAFSA [3], modern sprinkler heads have a RTI of 160 or less, whilst many 'quick response heads' have RTI ratings of 50

or less. Given this, the RTI rating used for this research was decided to be set at a constant of 40. FDS uses this value of RTI to control the activation of the sprinklers using equation (9). Within this, the gas temperature is represented as u, T_l, T_g and T_m are the link, gas and sprinkler mount temperatures, respectively. C and C_2 denote the C-Factor of the sprinkler, both empirical constants assigned at the default FDS setting of 0 and $6x10^6$, respectively.

$$\frac{dT_l}{dt} = \frac{\sqrt{|u|}}{RTI}(T_g - T_l) - \frac{C}{RTI}(T_l - T_m) - \frac{C_2}{RTI}\beta|u| \qquad \text{Eq. 9}$$

A full specification of how the boundary conditions were used within this study is shown in Table 2.

In order to collect data, 5 sensors have been placed symmetrically along the centre of the cabin aisle, spaced out evenly along the length of the cabin, all at a height of 1.5 m.

2.3 Meshing of the flow domain

Due to the geometrical extent of the railroad car and prior mentioned LES settings, each simulation within this study demanded a high amount of computational power. A nominal hexahedral element mesh size of 0.1 m was selected as an initial discretisation. To ascertain the accuracy of the predication produced by this mesh it was decided to decrease the element size by a third [22, 23]. A full simulation of each mesh was ran using the boundary conditions of simulation 1, detailed previously. The fine mesh discretion was used within the investigation based upon the two criteria. The first is that the computational power required to furtherly discretise the mesh was outweighed by the accuracy of the results produced. As the results within Table 3 show, there is an insignificant difference in temperature, in relation the objectives of this study, between the two analysed meshes. This would suggest that additional discretisation would in turn lead to further insignificant difference between mesh sizes, but however, exponentially increase the computational demand of the analysis. This was confirmed when in comparison to similar papers within this field, which have been published within reputable journals with coarser meshing [24,25].

Table 3. Mesh independence testing

Mesh	Number of elements	Element size (m)	Average temperature after 60 s	Average temperature after 120 s
Initial	216,000	0.1000	23.7128	22.4869
Fine	729,000	0.0667	23.8064	21.8279

3. Results and Discussions

The results section of this study has been divided into three parts for better comparative analyses. In the first sub-section, the fire is initiated and is allowed to spread within the passenger railroad car without the activation of the fire suppression system. In the second sub-section, fire is initiated and allowed to spread within the passenger railroad car however, the fire suppression system is activated based upon the specification of the root time index (RTI), as discussed within section. In this sub-section, the effects of hydrant's droplet size on fire suppression are investigated. The third sub-section resembles the second sub-section, with the difference that the effects of hydrant flow rate are investigated instead of droplet size.

3.1 Effects of fire propagation on the temperature distribution within the passenger railroad car

Figure 2 depicts the spatial and temporal variations in temperature within the passenger railroad car, after the initiation of fire. It can be clearly seen that in the first minute after fire initiation, it spreads vertically upwards, and the flames reach the roof of the car between 60 s and 85 s after fire starts. This subsequently leads to increase in ambient air's temperature in the upper sections of the car. This is due to the buoyancy of air; hot air rises due to decrease in its density. As time passes, heat transfer increases from the fire to the ambient air, further increasing its temperature. Due to wall effect (roof of the car), the hot air spreads laterally within the car until the partition walls on either ends of the car forces hot air to start accumulating within the car in the vertical direction. Thus, the thermal gradient in top-to-bottom direction is visible in the Figure 2. It is noteworthy here that after 135 s of fire initiation, the temperature of air in the upper section of the passenger railroad car has increased to more than 60°C and the temperature distribution is uniform in the lateral direction. At the elevation where normally peoples' head would be, the air temperature is more than 45°C.

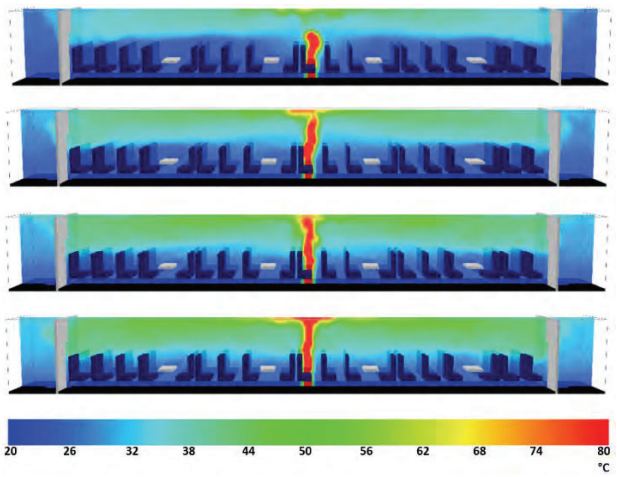

Figure 2. Temperature variations within the passenger railroad car after (a) 60 s (b) 85 s (c) 110 s and (d) 135 s for fire initiation

Further analysing the temperature distribution within the passenger railroad car, Figure 3 depicts variations in temperature on a cross-sectional plane at x=7m, which is approximately in the middle of fire and the left partition wall. The maximum scale in this Figure has been set to a lower temperature value for clarity; actual temperature surpasses 35°C. It can be seen that after 60 s on fire initiation, the thermal gradient along the height of the passenger railroad car is quite significant; the temperature in the lower section of the car is close to normal/comfortable temperature. As seen in Figure 3 (a), at this moment, the hot air is still propagating laterally and thus, the direction of flow is towards the partitioning wall. Once the hot air has reached the portioning wall, and there is no more

room available for lateral flow, build-up of hot air layers in the vertical direction. This is accompanied by reduction in the thermal gradient in Y direction, indicating that air inside the passenger railroad car is heating up quickly everywhere.

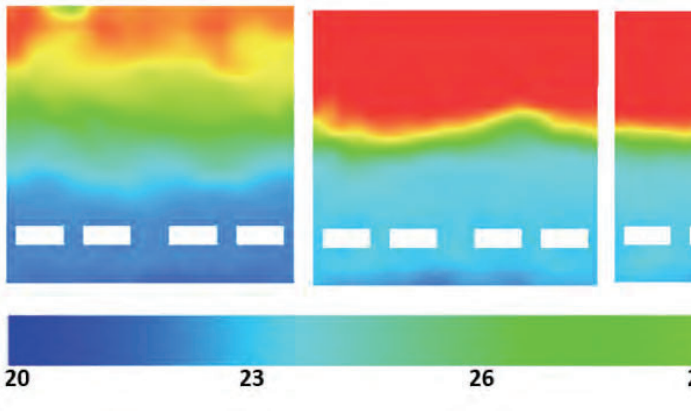

Figure 3. Temperature variations on the cross-sectional plane x=7m of the passenger railroad car after (a) 75 s (b) 85 s (c) 95 s and (d) 105 s of fire initiation

Figure 4 (a) depicts the temporal variations in the average temperature of sensors 1, 2, 4 and 5. Sensor 3 has been purposefully excluded from this as it is directly above the fire and thus, its temperature readings are considerably higher than the rest. Sensor 3 temperature data is shown in Figure 4(b) for reference. It is noteworthy that all the sensors are installed on the roof of the passenger railroad car and thus, this average temperature data is for the top section of the car only. It can be seen in Figure 4(a) that average temperature within the passenger railroad car increases after the initiation of fire. There are two distinct region (or patterns) that are observable here. From fire initiation till around 60 s, the increase in average temperature follows an almost linearly increasing path with a certain gradient. From 60 s to the end of the numerical simulation (i.e., 150 s after fire initiation), the rate of increase in the average temperature seems to be much higher. Till 60 s, the fire is still spreading, and the hot air is flowing laterally within the passenger railroad car. Once this hot air reaches the portioning walls, and starts accumulating in the vertical direction, the increase in temperature in the upper section of the car speeds up. The temperature data from sensor 3 in Figure 4(b) also confirms this; the temperature increases up to around 60 s after which, average temperature remains almost constant.

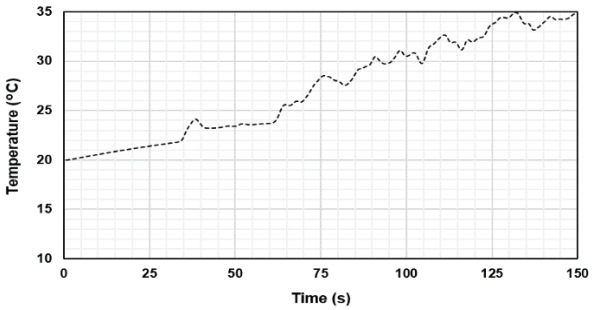

(a)

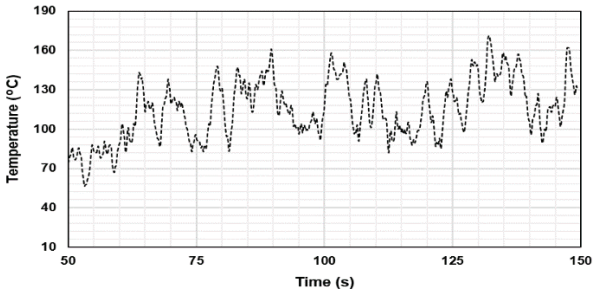

(b)

Figure 4. Average temperature recorded by (a) sensors 1, 2, 4 and 5 (b) sensor 3

Research studies have extensively reported that one of the primary causes of fatalities in case of fire incidents within enclosures is the suffocation i.e., lack of fresh, breathable air. This is because the fresh air is either replaced by or is heavily contaminated by soot particles, extensive inhalation of which causes severe respiratory diseases or even death. Hence, the present study would be incomplete without a thorough investigation on the concentration of soot particles within the passenger railroad car, which is shown in Figure 5. Expectedly, concentration of soot particles follows the same trend as the temperature distribution in Figure 2. Soot particles are concentrated in the fire and spread laterally along the passenger railroad car. After 104 seconds of fire initiation, it can be noticed that at head level, the concentration of soot particles is quite uniform, with a density of around 0.2 ppm.

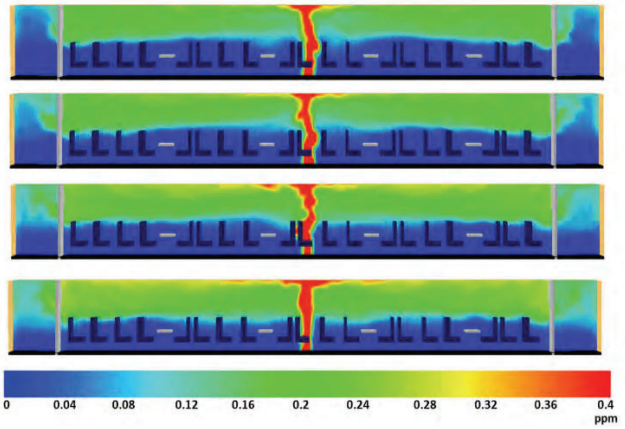

Figure 5. Concentration of soot particles within the passenger railroad car after (a) 72 s (b) 80 s (c) 94 s and (d) 104s

3.2 Effects of hydrant droplet size on the temperature distribution within the passenger railroad car

In order to design efficient fire suppression systems for enclosures, it is important to investigate the effects of different operational parameters of the system on fire suppression effectiveness. In this section of the present study, we analyse the effects of different hydrantdroplet sizes on fire suppression. Figure 6 depicts the spatio-temporal variations in temperature after the activation of the fire suppression system, for hydrant droplet sizes of 750 μm and 250 μm. The different time instances shown are 69-75 s, 80 s and 90 s after the initiation of fire, where the fire suppression system activates at 69 s. It can be seen that for both droplet sizes shown, the fire is gradually suppressed however, the fire suppression phenomenon is more pronounced in case of 250 μm droplets. It should be noted that the hydrant flow rate in both these cases is 300 l/min. So, the question arises;

why are smaller droplets more effective in fire suppression? This is explained in the section below.

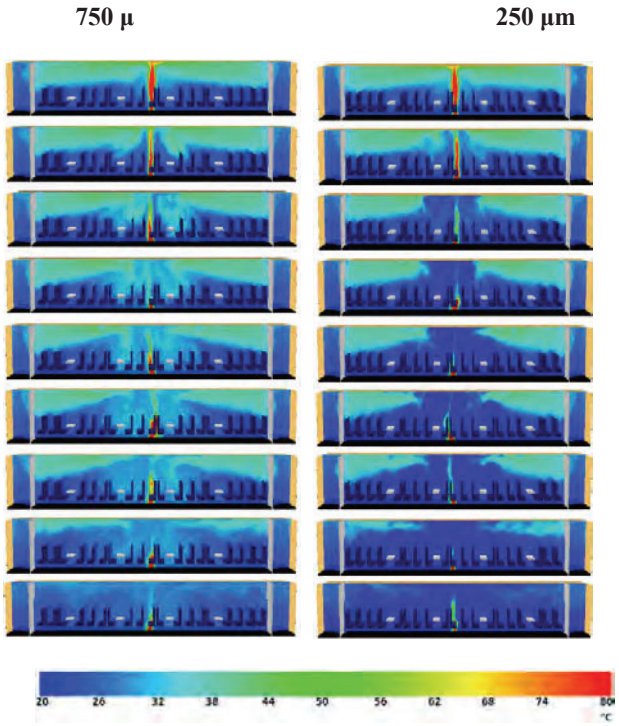

Figure 6. Temperature variations within the passenger railroad car after the activation of the fire suppression system for different hydrant droplet sizes**Table 4**. Surface area of droplets per second for 100 l/min flow rate

For 300 l/min	750 µm	250 µm
Number of droplets released per second	22,635,316	611,153,552
Surface area of each droplet	1.767×10^{-6} m^2	1.963×10^{-7} m^2
Surface area of all droplets per second	40 m^2	120 m^2

Newton's law of cooling states that the rate of heat transfer between two bodies in relative motion is proportional to the area through which heat transfer is taking place. In current context, if the surface area of the droplets is more, the heat transfer from fire to hydrant will be more. Comparing the surface area of a 750 µm droplet with the surface area of a 250 µm droplet, the former is 9 times higher, as shown in Table 4. However, there will be more than one droplet being released by the fire suppression system. Based on a fixed hydrant flow rate of 300 l/min, the number of 250 µm droplets released per second are 27 times more than the number of 750 µm droplets. The surface area (or heat transfer area) of 250 µm droplets is 3 times the surface area of 750 µm droplets. Thus, for the same heat transfer coefficient (in both cases the hydrant is the same i.e. water), the rate of heat transfer in case of 250 µm will be higher. Hence, the drop in air temperature within the passenger railroad carriage when hydrant of 250 µm droplet size is released will be higher compared to hydrant droplet size of 750 µm.

Similarly, on the cross-sectional plane at x =7m, it can be seen in Figure 7 that the fire suppression is faster when hydrant droplet size of 250 µm is used. After 75 s of fire initiation (i.e. 7 s after the activation of fire suppression system), the lower section of the passenger railroad car is largely cooled down to 20° for 250 µm droplets, while for 750 µm droplets, it's still above 25°C. Moreover, after 23 s of activation, the hydrant with droplet size of 250 µm has almost completely extinguished the fire, while in case of 750 µm droplets, it is still not completely extinguished even after 105 s.

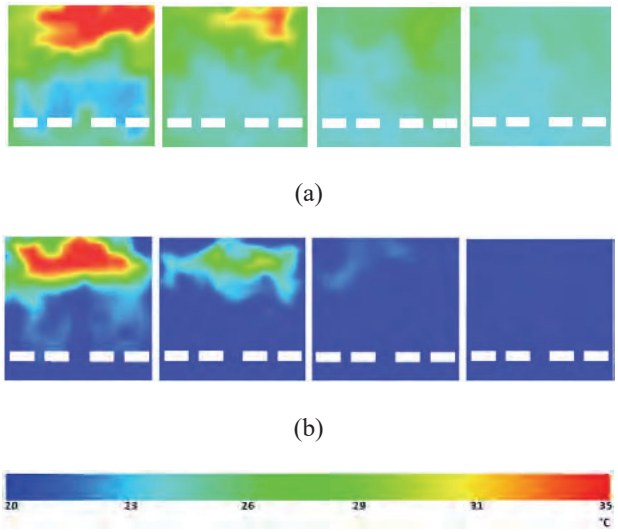

Figure 7. Temperature variations on the cross-sectional plane x=7m of the passenger railroad car after (a) 75 s (b) 85 s (c) 95 s and (d) 105 s of fire initiation for droplet sizes of (a) 750 µm and (b) 250 µm

Figure 8 depicts the temporal variations in the average temperature recorded by the sensors for different droplet sizes considered in the present study. For comparative analysis, data from Figure 4 is also included for reference. It can be clearly seen that the fire suppression system activates at around 69 s after fire initiation. Momentarily, most probably due to numerical instability/error, the average temperature of the sensors seems to be higher than the case when the fire suppression system remains deactivated. Thereafter, the average temperature rapidly drops irrespective of the droplet size. The smaller the droplet size, more reduction in the average temperature can be seen. For sensor 3 in Figure 8(b), as discussed in the previous sub-section, the temperature is too high to be compared against the temperature recorded by other sensors.

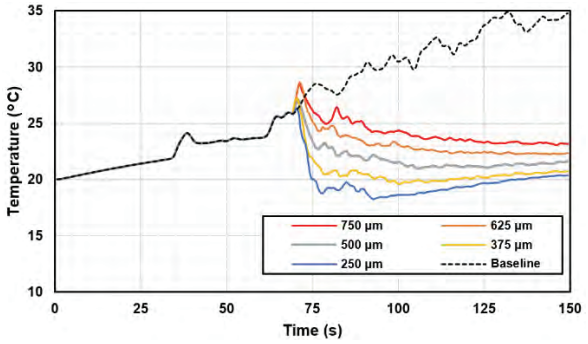

(a)

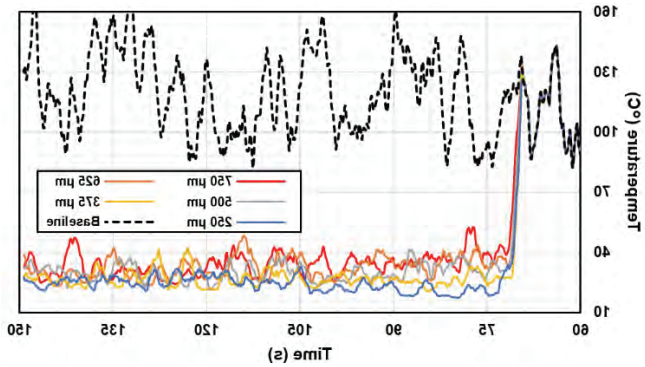

(b)

Figure 8. Comparison of average temperature recorded by (a) sensors 1, 2, 4 and 5 (b) sensor 3 for the different hydrant droplet sizes

Figure 9 depicts the soot particles concentration within the passenger railroad car after the activation of the fire suppression system, for hydrant droplet sizes of 750 µm and 250 µm. The different time instances shown in the Figure are 72 s, 80 s, 94 s and 104 s after the initiation of fire. In comparison with Figure 5, for both droplet sizes, the concentration of soot particles is considerably less, especially in the upper section of the car however, it is higher in the lower section. Moreover, there doesn't seem to be any significant difference between 750 µm and 250 µm hydrant droplet size when it comes to soot particles concentration. The possible reasons for these two observations can be explained through wet scavenging i.e. the ability of soot particles to attract and retain water droplets at high humidity [24]. When the fire suppression system is activated, there is a very high concentration of soot particles in the upper/top section of the passenger railroad car, as seen in Figure 5, along with high humidity due to release of hydrant droplets. Fresh soot particles, although mostly hydrophobic in nature [25], contain micropores on their surfaces that act as hydrophilic material [26] and thus, absorb the hydrant which leads to increase in their hygroscopicity [27, 28]. By consuming thermal energy from the fire, a significant amount of hydrant evaporates, leaving the soot particles in their current position i.e. in the upper section. The remaining hydrant (which hasn't evaporated), under the action of gravity and momentum from the hydrant jet flow, descends to the lower section of the passenger railroad car. Thus, a more uniform distribution of soot particles is expected within the passenger railroad car.

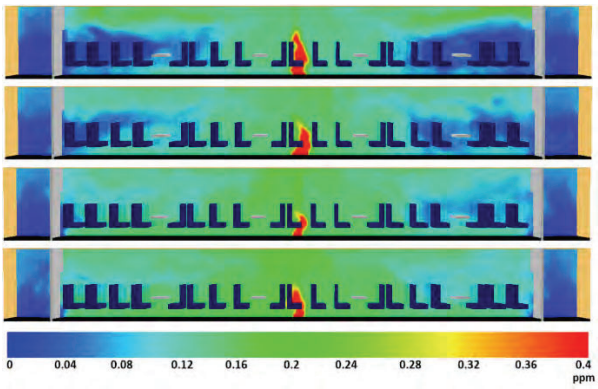

(a)

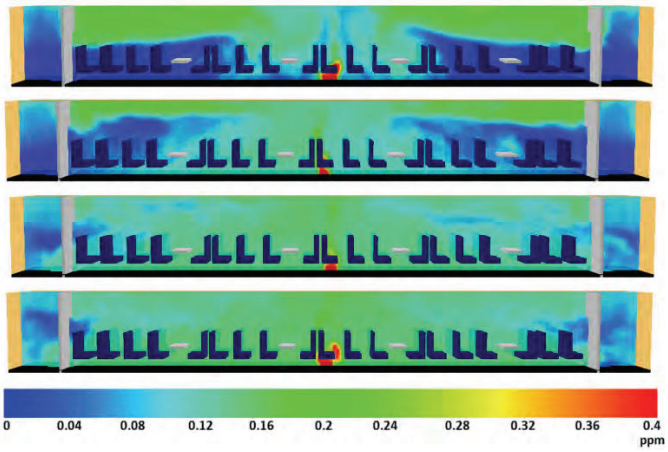

(b)

Figure 9. Concentration of soot particles within the passenger railroad car for hydrant droplet sizes of (a) 750 µm and (b) 250 µm

3.3 Effects of hydrant flow rate on the temperature distribution within the passenger railroad car

Hydrant flow rate is another key operational parameter of the fire suppression system. Investigations have been carried out on the effects of different hydrant flow rates, ranging from 300 l/min to 100 l/min in decrements of 50 l/min, on the suppression of fire within the passenger railroad car. Figure 10 depicts the spatial variations in temperature after 1 s, 2 s, 3 s, 4 s, 5 s, 6s, 11 s and 21 s of activation of fire suppression system, for hydrant flow rates of 300 l/min and 100 l/min. The droplet size considered in this investigation is kept constant at 750 µm, thus, a part of this Figure 10 (and the following figures in this sub-section) that relates to 300 l/min of hydrant flow rate are the same as presented in the previous sub-section; they have been included here again for comparative purposes only. It can be clearly seen in Figure 10 that as the hydrant flow rate increases, the fire suppression is more effective/quicker. According to the equation for the rate of heat transfer i.e., $\dot{Q} = \dot{m}C_p\Delta T$, as the hydrant mass flow rate (and volumetric flow rate as hydrant has a constant density) increases, the rate of heat transfer from the fire to the hydrant increases, resulting in its suppression. Thus, in case of 100 l/min flow rate, after 21 s of activation of the fire suppression system, the temperature within the railroad car is higher than for 300 l/min of hydrant flow rate, especially in the upper section of the car, as expected.

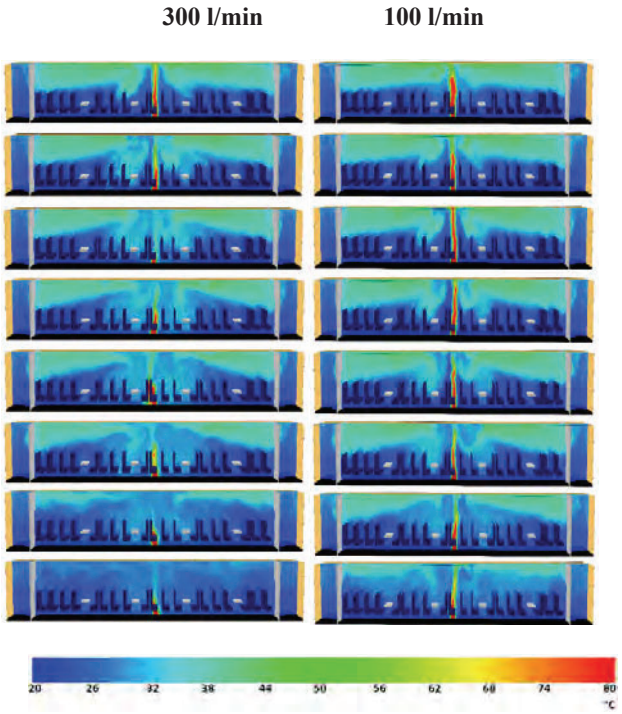

Figure 10. Temperature variations within the passenger railroad car after the activation of the fire suppression system for different hydrant flow rates

On the cross-sectional plane x =7m, it can be seen in Figure 11 that the fire suppression is more effective for 300 l/min of hydrant flow rate compared to 100 l/min. The temperature in the upper section of the plane drops rapidly for 300 l/min flow rate. It can be noticed that the temperature after 105 s of fire initiation (i.e., after 36 s of activation of the fire suppression system) is nearly uniform within the car for 300 l/min hydrant flow rate, while we still see temperature of around 32°C for 100 l/min flow rate. As the hydrant droplet size remains the same in both these cases, the number of droplets released per second are 22.6 million for 300 l/min and 7.5 million for 100 l/min, thus the combined surface area of droplets for 300 l/min is 3 times more than the combined surface area of droplets for 100 l/min hydrant flow rate, resulting in faster fire suppression for 300 l/min.

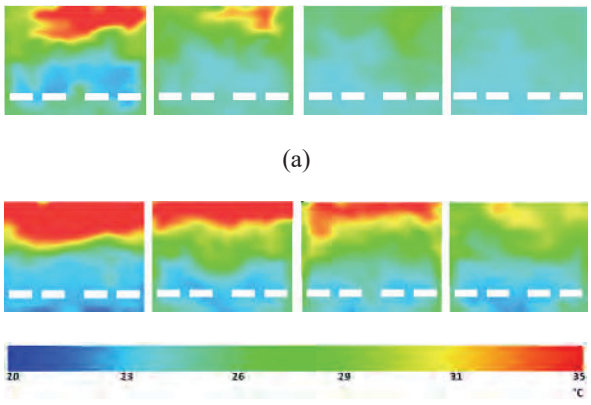

(a)

(b)

Figure 11. Temperature variations on the cross-sectional plane x=7m of the passenger railroad car after (a) 75 s (b) 85 s (c) 95 s and (d) 105 s of fire initiation for hydrant flow rates of (a) 300 l/min and (b) 100 l/min

Figure 12 depicts the temporal variations in the average temperature recorded by the sensors for different hydrant flow rates considered. It can be clearly seen in Figure 12 (a) that for sensors 1, 2, 4 and 5, the average temperature reaches 24°C for 300 l/min of hydrant flow rate, as compared to 27°C for 100 l/min. It is also noteworthy that with more hydrant flow available to suppress the fire, reaching steady state temperature takes more time and thus, for 300 l/min, the steady state temperature is reached at 125 s, while for 100 l/min, this is reached at 100 s.

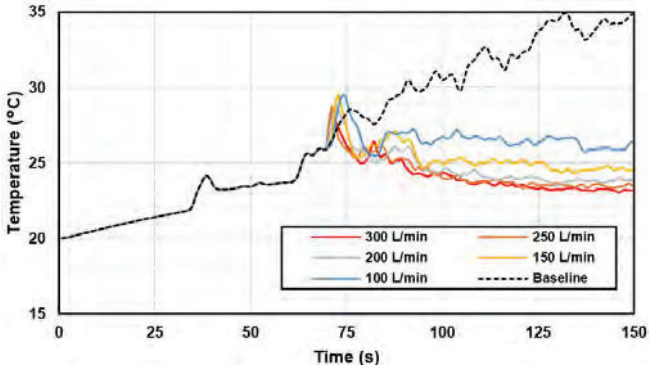

(a)

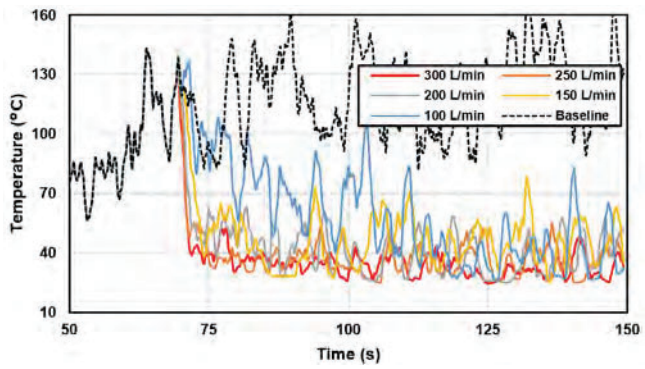

(b)

Figure 12. Comparison of average temperature recorded by (a) sensors 1, 2, 4 and 5 (b) sensor 3 for the different hydrant flow rates

Figure 13 depicts the soot particles concentration within the passenger railroad car after the activation of the fire suppression system, for hydrant flow rates of 300 l/min and 100 l/min respectively. In contrast to the effects of hydrant droplet size discussed in the previous sub-section, considerable difference can be seen between the two hydrant flow rates shown. For 300 l/min, the concentration of soot particles is significantly lower and more uniformly distributed within the passenger railroad car, compared to 100 l/min flow rate. This is because more hydrant is available for accumulation in the micropores of the soot particles compared to 100 l/min and thus, many particles descend towards the floor of the car. While in case of 100 l/min hydrant flow rate, due to less available hydrant (compared to 300 l/min), soot particles are more concentrated in the upper section of the car.

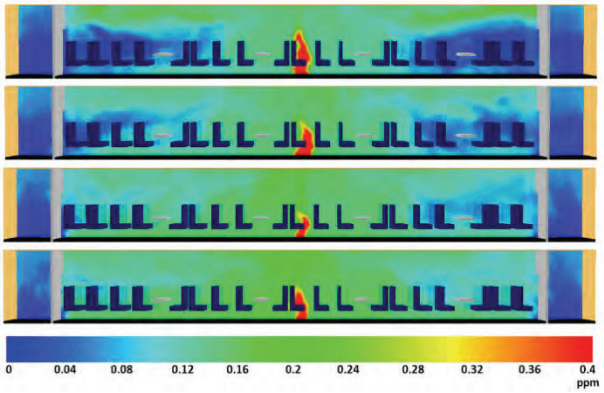

(a)

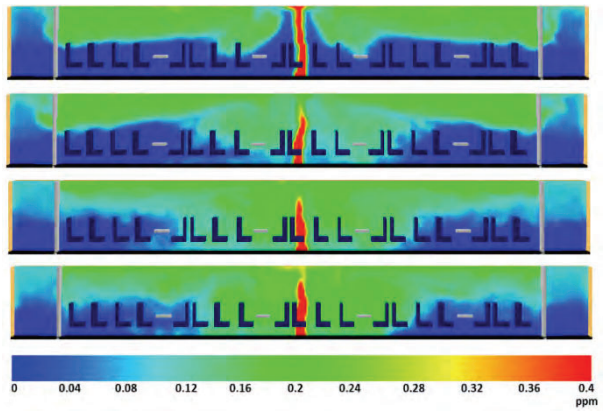

(b)

Figure 13. Concentration of soot particles within the passenger railroad car for hydrant flow rates of (a) 300 l/min and (b) 100 l/min

4. Conclusions

Based on the results presented in the present study, it can be concluded that smaller hydrant droplets are more effective in extinguishing the fire within the passenger railroad car for a given flow rate because of their larger surface/heat transfer area. Wet scavenging phenomena has been observed to occur within the car when the fire suppression system is activated, resulting in more uniform distribution of soot particles within the car. It has further been observed that as the flow rate of the hydrant increases, fire suppression is more effective. The results obtained in the present study can be used as guidelines for the development of efficient fire suppression systems for enclosures.

References

1. Efficiency and Effectiveness of Sprinkler Systems in the United Kingdom: An Analysis from Fire Service Data, National Fire Chiefs Council (NFCC), Birmingham, UK, 2019.
2. Frank, K. et al., 2013. A review of sprinkler system effectiveness studies, Fire Science Reviews, 2(6).
3. Craig, M. and Asim, T., 2020. Numerical investigations on the propagation of fire within a railway carriage, Energies 13(4999)
4. Chow, W.K.; Lam, K.C.; Fong, N.K.; Li, S.S.; Gao, Y.; Yeoh, G. Numerical Simulations for a Typical Train Fire in China. Modelling and Sim. in Eng. 2011, 2011, 1-7.
5. Guy Marlair, Jean-Christophe Le Coze, Woon-Hyung Kim. The Daegu metro fire: a review of technical and organisational issues. 2. International Symposium on Tunnel Safety and Security (ISTSS 2006), Mar 2006, Madrid, Spain. pp.15-25
6. King, T.Y., 1975. Smoke and carbon monoxide formation from materials tested in the smoke density chamber, Centre for fire research, pp. 5-11. Washington D.C.
7. Hostikka, S. and McGrattan, K., 2005. Numerical modelling of radiative heat transfer in water sprays. Fire safety journal, 41, pp.76-86.
8. Liu, H. et al. Critical assessment on operating water droplet sizes for fire sprinkler and water mist systems. Journal of Building Engineering 2020, 28.
9. Lal, S.; Gupta, M.; Kushari, A.; Kapoor, J.C.; Maji, S. Suppression of pool fire in a large enclosure with water mist. International Journal of Spray and Combustion Dynamics 2013, 5, 181-200.
10. Kooij, S.; Sijs, R.; Denn, M.M.; Villermaux, E.; Bonn, D. 2018. What determines the drop size in sprays? Physical review, 8, 3.
11. Fleming, R.P. 2020. Sprinkler hydraulics: A guide to fire system hydraulic calculations. 3edn. pp 19-25. Springer: Cham, Switzerland.
12. Li, J. 1996. Effect of pressure and nozzle shape on the characteristics of sprinkler droplet spectra, Journal of agricultural engineering research, 66, 15-21.
13. Lin, Z.; Bu, R.; Zhao, J.; Zhou, Y. Numerical investigation on fire-extinguishing performance using pulsed water mist in open and confined spaces. Case Studies in Thermal Engineering 2019, 13.
14. [14] RODRIGUEZ, S., 2019. Applied computational fluid dynamics and turbulence modelling, pp.197-223. Cham, Switzerland: Springer.
15. ANSYS® FLUENT, 2009. 23.3.13, Using the Rosin-Rammler Diameter Distribution Method, ANSYS, Inc.
16. Alderliesten, M., 2013. Mean Particle Diameters. Part VII. The Rosin-Rammler Size Distribution: Physical and Mathematical Properties and Relationships to Moment-Ratio Defined Mean Particle Diameters. Particle, 30(3), pp. 244-245.
17. McGrattan et al., 2021. Fire Dynamics Simulator User's Guide. 6eds, Gaithersburg, MD: NIST. pp.202-204.
18. McGrattan et al., 2021. Fire Dynamics Simulator Technical Reference Guide. 6eds, Gaithersburg, MD: NIST.
19. Liu, H. et al., 2020. Critical assessment on operating water droplet sizes for fire sprinkler and water mist systems. Jour. of building eng, vol 28.
20. Lawson, J.R., Walton, W.D. and Evans, D.D., 1988. Measurement of droplet size in sprinkler sprays. National bureau of standards, Gaithersburg, MD: US Dep. of Commerce
21. Pásztor, J. et al., 2020. Droplet size analysis of spray nozzles.
22. BAFSA., 2010. Information File: Sprinkler Heads. Issue 1.
23. D Singh, AM Aliyu, M Charlton, R Mishra, T Asim, AC Oliveira., 2020. Local multiphase flow characteristics of a severe-service control valve. Journal of petroleum science and engineering 195, 107557
24. D Singh, M Charlton, T Asim, R Mishra, A Townsend, L Blunt., 2020. Quantification of additive manufacturing induced variations in the global and local performance characteristics of a complex multi-stage control valve trim. Journal of petroleum science and engineering 190, 107053
25. Bilal Zuberi, Kirsten S. Johnson, Gretchen K. Aleks, Luisa T. Molina and Mario J. Molina (2005) Hydrophilic properties of aged soot; Geophysical Research Letters (32) L01807.
26. Laura Lintis, François-Xavier Ouf, Philippe Parent, Daniel Ferry, Carine Laffon and Cécile Vallières (2021) Quantification and prediction of water uptake by soot deposited on ventilation filters during fire events; Journal of Hazardous Materials (403) 123916.
27. Olga Popovicheva, Natalia M. Persiantseva, Natalia K. Shonija, Paul DeMott, Kirsten Koehler, Markus Petters, Sonia Kreidenweis, Victoria Tishkova, Benjamin Demirdjian and Jean Suzanne (2008) Water interaction with hydrophobic and hydrophilic soot particles; Physical Chemistry Chemical Physics (10) 2332-2344.
28. S. Henning, M. Ziese, A. Kiselev, H. Saathoff, O. Möhler, T. F. Mentel, A. Buchholz, C. Spindler, V. Michaud, M. Monier, K. Sellegri and F. Stratmann (2012) Hygroscopic growth and droplet activation of soot particles: uncoated, succinic or sulfuric acid coated; Atmospheric Chemistry and Physics (12) 4525-4537.
29. X Liu, T Asim, G Zhu, R Mishra., Theoretical and experimental investigations on the combustion characteristics of three components mixed municipal solid waste. Fuel 267, 117183.